


PRL3-zumab as an anti-angiogenic therapy in neovascular eye diseases

Received: 28 February 2024

Accepted: 8 May 2025

Published online: 23 May 2025

 Check for updates

Koon Hwee Ang¹, Min Thura¹, Queenie Shu Woon Tan¹, Abhishek Gupta¹, Kam Yew Kuan¹, Jie Li¹, Pei Ling Chia¹, Beiying Qiu², Jimmy Ming Hong³, Ke Guo¹, Xiaomeng Wang^{1,2,3}, Xinyi Su^{1,3,4,5} & Qi Zeng^{1,6} 

Neovascular eye diseases represent a major cause of irreversible blindness. Here, we report the specific upregulation of endogenous PRL3 protein in diseased choroid-RPE in choroidal neovascularization (CNV) mouse model (male), and diseased retina in oxygen-induced retinopathy (OIR) mouse model (mixed gender), indicating PRL3's role in neovascularization. Intravenous (IV) delivery of anti-PRL3 antibody in CNV model demonstrates superior efficacy in reducing vascular leakage compared to intravitreal (IVT) route due to larger dose permitted by IV. VEGF treatment upregulates endogenous PRL3 protein in human retinal microvascular endothelial cells (HRMECs). Retroviral PRL3 overexpression in HRMECs promotes endothelial proliferation, migration and permeability by facilitating the phosphorylation of ERK1/2, AKT, Paxillin and SRC. However, VEGF-induced proliferation is absent in PRL3-knockout HRMECs. PRL3-zumab, an anti-PRL3 humanized monoclonal antibody, has shown a strong safety profile in ongoing multi-national Phase II trials as an intravenous-administered cancer immunotherapeutic. PRL3's involvement in ocular pathological angiogenesis suggests the potential of repurposing PRL3-zumab to treat neovascular eye diseases.

Angiogenesis is the process of new blood vessel formation from pre-existing ones. Neovascular eye diseases are characterized by the overgrowth of aberrant blood vessels and vascular leakage which lead to the deterioration of vision. According to the first World Report on vision by the World Health Organization in 2019, there were 196 million age-related macular degeneration (AMD) patients and 146 million diabetic retinopathy/diabetic macular edema (DR/DME) patients globally¹ and the figures are set to rise due to an aging population in many countries. Visual impairment is debilitating to patients and causes huge economic and social burdens for many societies.

In the 1990s, vascular endothelial growth factor (VEGF) was identified as the key molecule responsible for the pathogenesis of neovascular AMD (nAMD) and DR/DME^{2–4}. In the context of nAMD and DR/DME, various molecular mechanisms associated with aging and diabetes can lead to a reduction in retinal blood supply. Consequently, ocular cells (such as retinal pigment cells) are subjected to hypoxia and secrete VEGF, which promotes the formation of hyperpermeable vasculature. The resultant vascular leakage contributes to the occurrence of nAMD and DR/DME^{5,6}. So far, several anti-VEGF drugs have been approved by the US Food & Drug Administration (FDA). These anti-VEGF therapies

¹Institute of Molecular and Cell Biology (IMCB), Agency for Science, Technology and Research (A*STAR), 61 Biopolis Drive, Singapore 138673, Singapore.

²Centre for Vision Research, Duke NUS Medical School, 8 College Road, Singapore 169857, Singapore. ³Singapore Eye Research Institute (SERI), The Academia, 20 College Road, Level 6 Discovery Tower, Singapore 169856, Singapore. ⁴Department of Ophthalmology, Yong Loo Lin School of Medicine, National University of Singapore, Singapore 119260, Singapore. ⁵Department of Ophthalmology, National University Hospital, Singapore 119074, Singapore.

⁶Department of Biochemistry, Yong Loo Lin School of Medicine, National University of Singapore, Singapore 119260, Singapore.

✉ e-mail: mcbezengq@imcb.a-star.edu.sg

have been developed to suppress vascular leakage and have achieved considerable success in improving vision in some patients. Notable drugs include pegaptanib sodium, bevacizumab (off-label use), ranibizumab, aflibercept, brolucizumab and faricimab – a bispecific antibody targeting VEGF-A and Ang-2 that was very recently approved in 2022^{7–11}. Anti-VEGF antibodies (bevacizumab, ranibizumab and brolucizumab) and a selective VEGF antagonist (pegaptanib sodium) bind to secreted VEGF in the interstitial space and prevent the binding of VEGF-to-VEGF receptors on the endothelial cell surface, thereby reducing the formation of abnormal and leaky blood vessels. Aflibercept and conbercept are recombinant fusion proteins which function as decoy receptors for VEGF. Both are multi-targeted trap of VEGF and placental growth factor (PIGF) and these confer a strong angiogenic inhibition. In most cases, repeated administration of antibodies is required to ensure disease regression^{12,13}. However, according to clinical data published in recent years, a significant proportion of patients (~37% to 45% for nAMD and ~40% for DR/DME) do not respond well to anti-VEGF treatments^{14–16}. For instance, nAMD patients who are poor responders to anti-VEGF therapies develop persistent fluid exudation, new or unresolved hemorrhage, progressive lesion fibrosis and suboptimal vision recovery¹⁷. A significant proportion of DME patients has also been found to develop vitreoretinal fibrosis after treatment with bevacizumab due to the shift in balance between VEGF and connective tissue growth factor (CTGF)^{18,19}. Furthermore, as VEGF plays a key role in physiological angiogenesis and neuronal biology, there are potential safety concerns for long-term anti-VEGF therapy^{20,21}, particularly for patients with pre-existing conditions such as ischemic heart disease and stroke. Thus, there is an urgent need to discover an alternative target involved in VEGF signaling, which could be targeted to achieve equivalent efficacy, yet with reduced toxicity. Another concern for anti-VEGF treatment is its delivery via the intravitreal (IVT) route. IVT administration comes with its inherent ocular and systemic risks – ocular complications include damage to surrounding structures leading to traumatic cataracts, retinal tears, retinal pigment epithelium (RPE) tears, or even endophthalmitis which can be vision-threatening²², and systemic risks associated with anti-VEGF treatment includes stroke and myocardial infarction, both of which may be life-threatening. A safer alternative route of administration could potentially alleviate these risks for nAMD and DR/DME patients.

Ocular angiogenesis and immune cell activation are highly related. Significant elevation of immune cells (monocytes and neutrophils) has been detected in peripheral circulation and choroidal vasculature of nAMD patients^{23,24}. In pathological conditions like nAMD or DR/DME, the immune cells initiate as a precursor for the pro-inflammatory reaction, which promotes angiogenesis^{24,25}. The hyperpermeable nature of the new blood vessels and local inflammatory response further activate the recruitment and infiltration of immune cells to the retinal tissue²⁶. Normalizing the leakiness in these abnormal blood vessels could be a way to reduce further worsening of these eye diseases.

PRL3 (Phosphatase of Regenerating Liver 3) is a cancer-associated phosphatase that is overexpressed in a wide repertoire of cancer types^{27,28}. PRL3 has been shown to be an oncogenic driver that regulates the hallmark traits of cancer cell biology, such as tumorigenesis and metastasis²⁹. We have previously developed an anti-PRL3 mouse monoclonal antibody³⁰ and demonstrated strong anti-cancer efficacy of anti-PRL3 antibody in mouse tumor models^{31,32}. A First-in-Class humanized monoclonal antibody drug against PRL3, named PRL3-zumab, was then developed³³. Thura et al reproducibly demonstrated the ability of PRL3-zumab to inhibit tumor growth^{28,33,34} and prevent relapse³⁴ in various preclinical mouse tumor models. In 2017, PRL3-zumab entered Phase I clinical trials in Singapore. Intravenous (IV) administration of PRL3-zumab has demonstrated a strong safety profile without drug-related severe toxicities or death³⁵. PRL3-zumab has since progressed to Phase II multi-national clinical trials as a therapy for advanced gastric and liver cancers in Singapore³⁶ and for advanced solid tumors in USA³⁷, China³⁸ and Malaysia.

Besides regulating the biological functions of cancer cells, PRL3 has been shown to play a role in tumor angiogenesis. This was first reported in 2004 by Guo et al, who demonstrated that EGFP-PRL3 overexpressing Chinese Hamster Ovary (CHO) cells could form micro- and macro-metastases which sprout into blood vessels³⁹. In the same year, Parker et al showed PRL3 expression in the vasculature of invasive breast cancers and PRL3 could promote endothelial migration in vitro⁴⁰. Additionally, in 2006, Guo et al found that PRL3 initiates tumor angiogenesis by recruiting endothelial cells via IL4 attenuation⁴¹. The proangiogenic role of PRL3 in tumor development has been well defined. Interestingly, *PRL3* mRNA expression in Human Umbilical Vein Endothelial Cells (HUVECs) is upregulated upon VEGF treatment through transcription factor MEF2C⁴² and PRL3 can facilitate VEGF signaling in endothelial cells via SRC⁴³, thereby demonstrating the relationship between PRL3 and VEGF. Since VEGF is implicated in the pathogenesis of various angiogenesis-driven diseases, it suggests that PRL3 could potentially mediate angiogenesis in other diseases beyond cancer. Hence, we were prompted to explore the potential role of PRL3 in other angiogenesis-driven diseases, such as neovascular eye diseases.

Results

PRL3 is co-expressed with CD31 and Ter119 in embryonic blood vessels and is involved in blood vessel remodeling in tumors

PRL3 has been reported to be expressed in pre-erythrocytes, fetal heart, and small developing blood vessels, but not in the mature counterparts⁴¹. We confirmed this observation by whole mount mouse E9.5 embryo staining of CD31⁺/Ter119⁺ blood vessels, which have co-expression of PRL3, but not its close homolog, PRL1 (Fig. 1a), indicating that PRL3 plays a role in embryonic angiogenesis during which VEGF level is high⁴⁴. A closer look at the PRL3⁺ tumor vasculature revealed a significantly lower pericyte coverage (lower % of CD31⁺αSMA⁺/CD31⁺ blood vessels) in PRL3⁺ tumors than in PRL3⁻ tumors ($p < 0.001$) (Fig. 1b–e). PRL3⁺ tumors also had a higher mean CD31⁺ microvessel density than PRL3⁻ tumors ($p < 0.001$) (Fig. 1b–d). Blood vessels with a reduced pericyte coverage could be immature and hyperpermeable or leaky^{41,45,46}. Hence, the significant reduction in pericyte coverage of the blood vessels in PRL3⁺ tumors suggest that these blood vessels could be hyperpermeable and nonfunctional (Fig. 1f). As neovascular eye diseases are caused by the abnormal growth of hyperpermeable blood vessels and vascular leakage, we postulated that PRL3 could be involved in the pathogenesis of neovascular eye diseases.

PRL3 protein is specifically overexpressed in mouse ocular tissues with excessive pathological angiogenesis

Laser-induced choroidal neovascularization (CNV) and oxygen-induced retinopathy (OIR) mouse models are commonly used to recapitulate nAMD and some features of DR/DME in humans, respectively⁴⁷. Specifically, nAMD is a choroidal disease while DR/DME is a retinal disorder. Western blotting of retinas and choroidal-RPE tissues harvested from C57BL/6 mice subjected to laser-induced CNV after a week showed that PRL3 expression is upregulated specifically in the diseased choroid-RPE complex but not in retina (Fig. 2a and c). In the OIR model, retinal neovascularization reaches its highest level at postnatal day 17 (P17)⁴⁸. Consistent with reports that PRL3 is expressed in developing neovessels⁴¹, western blotting revealed PRL3 expression in the retinas of P17 normal untreated control. Intriguingly, PRL3 is further induced in the retinas of P17 pups subjected to OIR (Fig. 2b and d). Localisation of PRL3 in CD31⁺ blood vessels was observed in the CNV lesion of Choroid-RPE flatmount (Supplementary Fig. 1, panel F). The association of PRL3 protein upregulation with the respective diseased ocular tissues indicates the potential involvement of PRL3 in pathological neovascularization in the eye and PRL3 could be a target for therapeutics development for neovascular eye diseases. Importantly, PRL3 is absent in normal human tissues such as liver, lung,

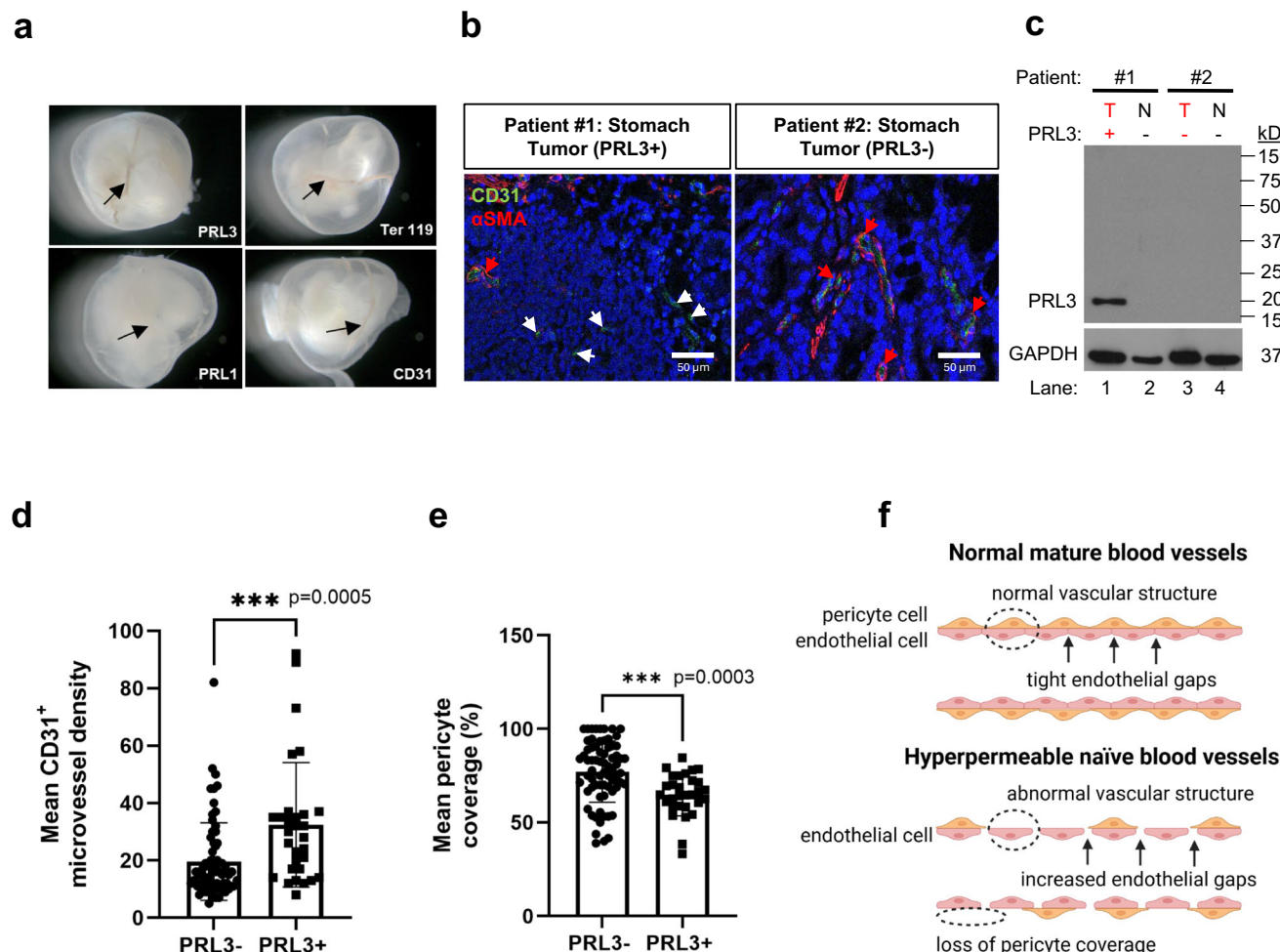


Fig. 1 | PRL3 (but not PRL1) is associated with embryonic angiogenesis and blood vessels in PRL3⁺ tumors have reduced pericyte coverage compared to those in PRL3⁻ tumors. **a** Whole mouse embryo staining shows that CD31/Ter119⁺ embryonic blood vessels express PRL3 but not PRL1, a close homolog. **b** Representative immunofluorescence images of PRL3⁺ (Patient #1) and PRL3⁻ (Patient #2) human stomach tumor sections stained with CD31 (green) and αSMA (red). Red arrows indicate CD31⁺αSMA⁺ blood vessels while white arrows indicate CD31⁺αSMA⁻ blood vessels. Scale bar, 50 μm. **c** Western blot of PRL3 protein expression of PRL3⁺ (lane 1) and PRL3⁻ (lane 3) stomach tumor sections shown in **b**. 'T' represents stomach tumor, and 'N' stands for patient-matched normal stomach tissue. Glyceraldehyde 3-phosphate dehydrogenase (GAPDH) served as a loading control. **d** Quantification of mean CD31⁺ microvessel density in tumor sections in **b**. *** $p=0.0005$. **e** Quantification of mean pericyte coverage in tumor sections in **b**. Blood vessels in PRL3⁺ tumors have a lower mean percentage of pericyte coverage compared to those in PRL3⁻ tumors ($p=0.0003$). **f** Schematic comparison of normal mature blood vessels and hyperpermeable naïve blood vessels (Created in BioRenderTM). All images shown are representative and the mean value was calculated by two-sided Student's *t* test (mean \pm s.d., $n \geq 3$ biologically independent samples each). *** $P < 0.001$. PRL3⁺ tumors ($n=7$ biological replicates and total of 70 10X images): $n=3$ colon; $n=4$ stomach; PRL3⁻ tumors ($n=3$ biological replicates and total of 30 10X images): $n=2$ colon; $n=1$ stomach. Source data are provided as a Source Data file.

colon, breast, stomach, thyroid, pancreas, kidney, prostate gland and bladder²⁸. Therefore, we anticipate that PRL3 therapeutics would cause negligible toxicity.

IV allows for a higher dose of anti-PRL3 antibody than IVT which translates to an enhanced efficacy in the recovery of CNV lesions

Next, we investigated the efficacy of anti-PRL3 antibody treatment on laser-induced CNV lesions using two routes of administration – intravitreal (IVT) or intravenous (IV) injections. By comparing the area of vascular leakage on Day 1 (before treatment) and Day 7 (6 days post treatment), anti-PRL3 antibody treatment by IVT administration (IVT: a single dose of 2.5 μg in 1 μL) led to an improved recovery of the CNV lesions compared to PBS/IgG group (anti-PRL3 ab: 35.1% versus PBS/IgG: 22.2%) (Fig. 3a–c). Aflibercept (Eylea) is one of the standard-of-care anti-VEGF treatments and was used as a positive control. IVT delivery of anti-PRL3 antibody was shown to be effective and its efficacy was comparable to aflibercept (Eylea) (Aflibercept: 38.1% versus anti-PRL3 ab: 35.1%).

PRL3⁺ tumors have a higher mean microvessel density than PRL3⁻ tumors ($p=0.0005$). **e** Quantification of mean pericyte coverage in tumor sections in **b**. Blood vessels in PRL3⁺ tumors have a lower mean percentage of pericyte coverage compared to those in PRL3⁻ tumors ($p=0.0003$). **f** Schematic comparison of normal mature blood vessels and hyperpermeable naïve blood vessels (Created in BioRenderTM). All images shown are representative and the mean value was calculated by two-sided Student's *t* test (mean \pm s.d., $n \geq 3$ biologically independent samples each). *** $P < 0.001$. PRL3⁺ tumors ($n=7$ biological replicates and total of 70 10X images): $n=3$ colon; $n=4$ stomach; PRL3⁻ tumors ($n=3$ biological replicates and total of 30 10X images): $n=2$ colon; $n=1$ stomach. Source data are provided as a Source Data file.

Since IV administration of anti-PRL3 antibody has shown an excellent safety profile in mice and human subjects, we investigated the therapeutic efficacy of this route of drug administration. The dosing schedule was similar to the anti-PRL3 antibody regimen used in the cancer model, which is two doses of 100 μg per week³². IV administration of anti-PRL3 antibody demonstrated a superior efficacy compared to PBS/IgG control (anti-PRL3 antibody: 65.3% versus PBS/IgG: -67.7%) and was 86% better than IVT treatment of anti-PRL3 antibody (IV: 65.3% versus IVT: 35.1%, $p=0.003$) due to the larger dose permitted by IV route (Fig. 3b–c). This is a proof-of-concept that targeting PRL3 is a viable treatment modality in neovascular eye diseases.

Vascular leakage could be caused by various mechanistic pathways, one of which is the VEGF-induced phosphorylation of SRC⁴⁹. Western blotting of choroid-RPE tissues showed that anti-PRL3 antibody treatment attenuates the phosphorylation of SRC, which could restore vessel integrity in the CNV lesions (Fig. 3d, Supplementary

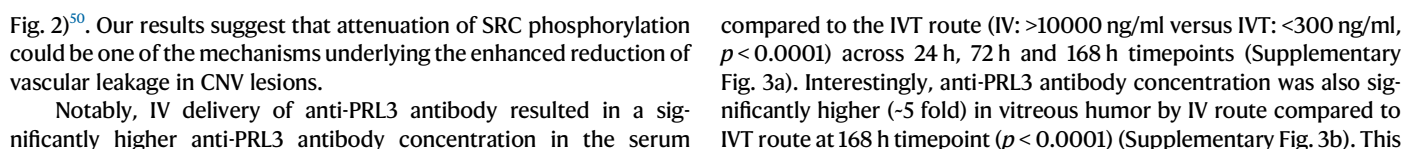


Fig. 2 | PRL3 is overexpressed in diseased choroid-RPE of CNV and diseased retina of OIR mouse models respectively. **a** Western blotting (WB) shows specific PRL3 overexpression in diseased choroid-RPE of CNV model (8-week mice) but not in those of untreated control (UT CTL). **b** WB shows specific PRL3 upregulation in the diseased retina of OIR model (17-day pups) but minimal in those of UT CTL. **c** Quantification of **a** ($p = 0.001$). **d** Quantification of **b** ($p = 0.0004$). Glyceraldehyde 3-phosphate dehydrogenase (GAPDH) and beta-Actin (β -Actin) served as loading controls. B16F0 and B16F10 are positive and negative controls for PRL3

immunoblot, respectively. All images shown are representative and the mean value was calculated by two-sided Student's t -test (mean \pm s.d., $n \geq 3$ biologically independent samples each; 8-week-old mice: UT CTL ($n = 6$) vs CNV ($n = 35$) and 17-day pups: UT CTL ($n = 11$) vs OIR ($n = 18$), *** $P < 0.001$). The samples analysed were derived from the same experiments and the blots were processed in parallel. R Retina, C choroid-RPE, UT CTL Untreated Control, CNV Choroidal neovascularization mouse model, OIR Oxygen-induced retinopathy mouse model. Source data are provided as a Source Data file.

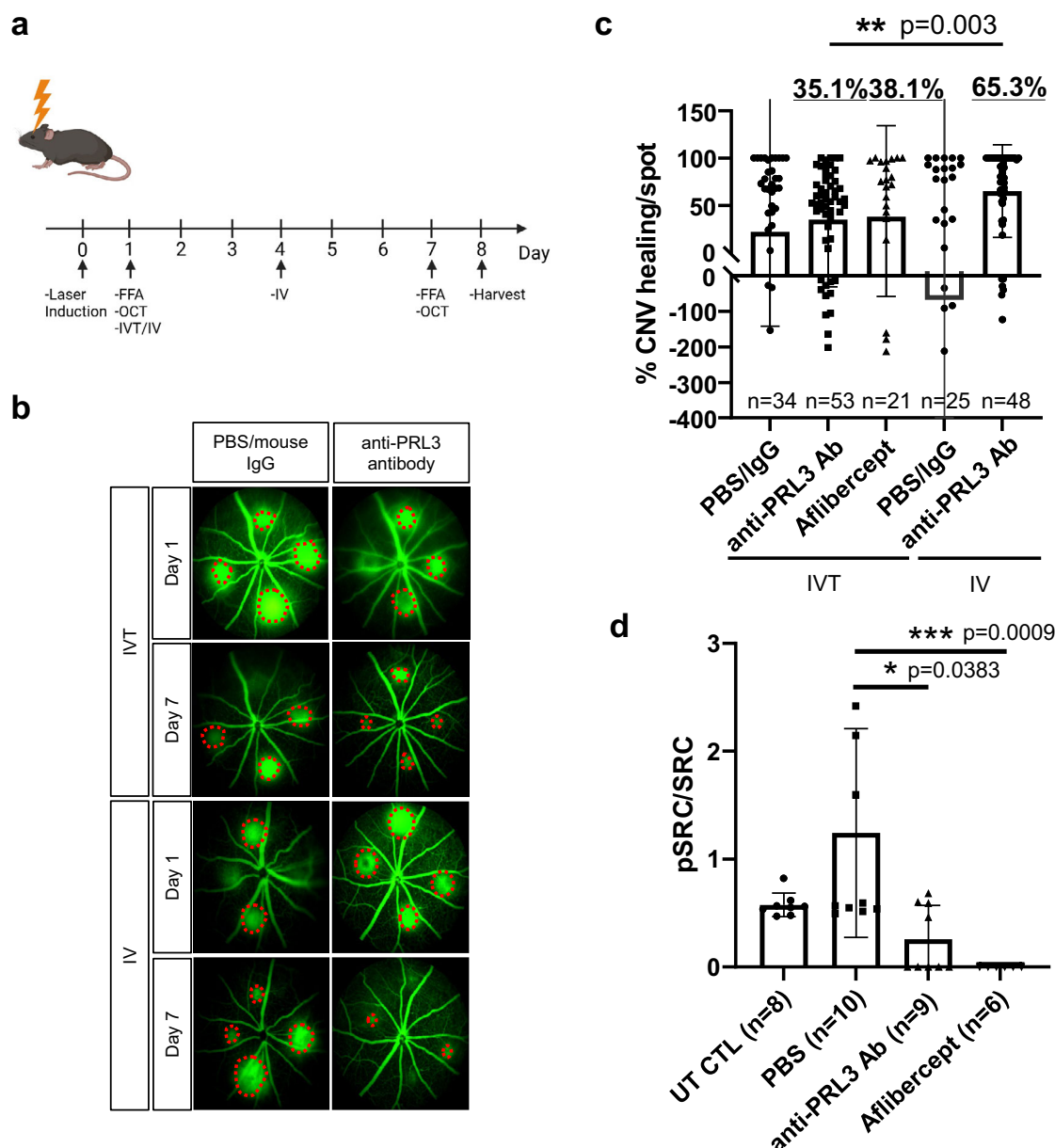


Fig. 3 | Superior efficacy of intravenous (IV) to intravitreal (IVT) delivery of anti-PRL3 antibody in the recovery of CNV lesions by attenuating SRC phosphorylation. **a** Experimental timeline of drug treatment (IVT and IV) in laser-induced CNV model. (Created in BioRender⁷²). **b** Representative FFA images of PBS/mouse IgG and anti-PRL3 antibody treated groups with IVT and IV as delivery routes (Day 7 versus Day 1). **c** Quantification of the % recovery of the CNV lesions after drug treatment. IV treatment of anti-PRL3 antibody showed significant recovery of CNV lesions compared to PBS/IgG control group (anti-PRL3 antibody: 65.3% versus PBS/IgG: -67.7%) and 86% better than IVT delivery of anti-PRL3 antibody (IV: 65.3% versus IVT: 35.1%, $p = 0.003$). Efficacy of IVT treatment of anti-

PRL3 antibody is comparable to that of aflibercept (Aflibercept: 38.1% versus anti-PRL3 antibody: 35.1%). 'n' indicates the number of CNV spots used in analysis. **d** Quantification of the Western blots of choroid-RPE tissues shows the attenuation of SRC phosphorylation (Y416) effected by anti-PRL3 antibody ($p = 0.0383$) and aflibercept ($p = 0.0009$) treatments. All images shown are representative and the mean value was calculated using one-way analysis of variance (ANOVA) (mean \pm s.d., $n \geq 3$ biologically independent samples each). *** $P < 0.001$; ** $P < 0.01$; * $P < 0.05$. FFA Fundus Fluorescein Angiography, OCT Optical Coherence Tomography, IVT Intravitreal, IV Intravenous. Source data are provided as a Source Data file.

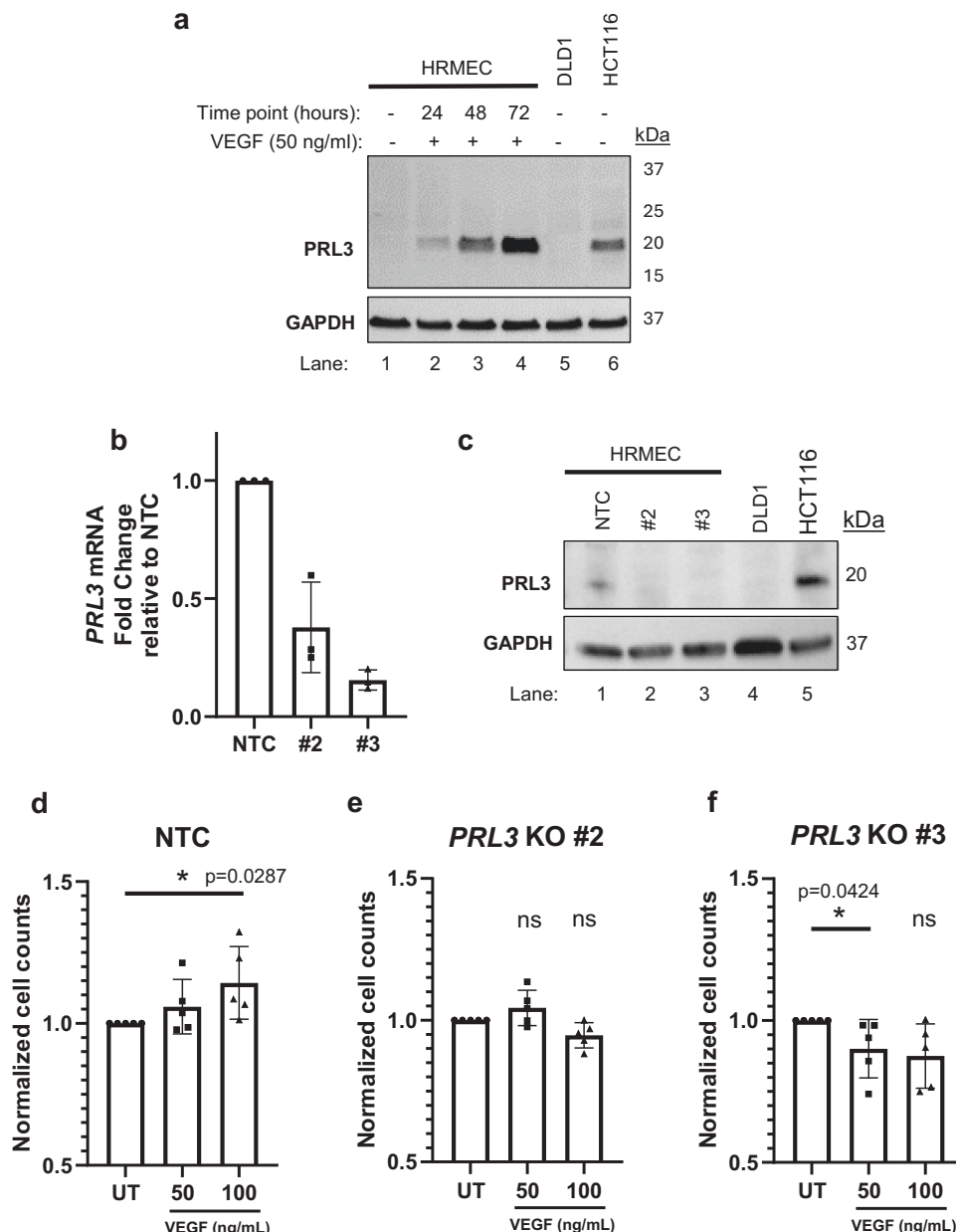


Fig. 4 | VEGF upregulates endogenous PRL3 protein that plays a role in VEGF-induced endothelial proliferation. **a** VEGF upregulates PRL3 protein expression in HRMECs in a time-dependent manner (highlighted in blue box) at which 72 h incubation results in the highest PRL3 expression ($n = 3$). **b** qPCR and **(c)** Western blotting analyses of PRL3 CRISPR KO HRMECs show diminished PRL3 mRNA and protein in #2 and #3 KO HRMECs ($n = 3$ replicates, pooled from three independent batches of transduced HRMECs). **d** In NTC control cells, VEGF treatment promoted dose-dependent endothelial proliferation at 50 ng/ml and 100 ng/ml in 48 h ($n = 5$ replicates, pooled from three independent batches of transduced HRMECs).

e–f However, this enhancement in proliferation was not observed in PRL3 KO HRMECs (#2 and #3) ($n = 5$ replicates, pooled from three independent batches of transduced HRMECs). The mean value was calculated using one-way analysis of variance (ANOVA) (mean \pm s.d., $n \geq 3$ replicates each). * $p < 0.05$, ns: not significant. Glyceraldehyde 3-phosphate dehydrogenase (GAPDH) served as a loading control. DLD1: PRL3⁺ Human colorectal cancer cells (negative control); HCT116: PRL3⁺ Human colorectal cancer cells (positive control). NTC: Non-Targeting Control, UT: Untreated Control. Source data are provided as a Source Data file.

correlated with the significantly improved efficacy of IV treatment compared to IVT delivery of anti-PRL3 antibody. It is also observed that by IV administration, there was a higher anti-PRL3 antibody concentration in the vitreous compartment of mice with laser-induced CNV lesions compared to that of normal mice without CNV lesions (CNV: 4608 ng/ml versus no CNV: 1390 ng/ml, $p < 0.0001$). This shows that the induction of CNV lesions by laser injury and compromise of Bruch's membrane could facilitate the leakage and influx of anti-PRL3 antibody, administered via IV, from blood circulation into the vitreous compartment (Supplementary Fig. 4).

VEGF upregulates endogenous PRL3 protein in HRMECs

Due to blood vessel abnormality caused by various factors such as aging and diabetes, ocular cells could experience hypoxia, thereby stimulating the secretion of VEGF to promote angiogenesis^{51,52}. To mimic this diseased angiogenic eye condition in humans, we treated HRMECs with recombinant VEGF protein in vitro. We found that VEGF treatment (50 ng/ml) upregulated endothelial PRL3 expression in a time-dependent manner. Treatment of VEGF (50 ng/ml) at 24 h, 48 h and 72 h timepoints showed that PRL3 expression was highest at 72 h (Fig. 4a). Given that VEGF is important for the causation of neovascular

eye diseases, PRL3 upregulation induced by VEGF provides critical evidence for the relevance of targeting PRL3 as a therapeutic strategy in neovascular eye diseases.

Furthermore, VEGF-induced PRL3 upregulation in HRMECs is transcriptionally regulated by MEF2C (Supplementary Fig. 5a–c), consistent with previous literature⁵³. PRL3 KO HRMECs were generated using CRISPR technology (Fig. 4b, c). VEGF stimulation did not enhance the proliferation of PRL3-depleted HRMECs, indicating that PRL3 plays an important role in VEGF-induced proangiogenic effects (Fig. 4d–f). Additionally, PRL3-zumab treatment inhibited VEGF-induced signaling in HRMECs by downregulating pSRC and pERK1/2, similar to bevacizumab treatment, in which pERK1/2 was reduced (Supplementary Fig. 6)

PRL3 overexpression promotes HRMEC proliferation, migration and permeability via enhanced proangiogenic signaling

To investigate the role of PRL3 in ocular endothelial biology, HRMECs stably expressing PRL3 (HRMEC-PRL3) were generated using retroviral transduction. Endothelial PRL3 overexpression promoted HRMEC proliferation (Fig. 5a, mean fold change = 1.3 ± 0.35 , $p = 0.018$) and migration (Fig. 5b, HRMEC-PRL3: 106.7 ± 46.8 versus HRMEC-Vector: 52.7 ± 36.5 , $p = 0.0499$) after 24 h. Interestingly, the HRMEC-PRL3 monolayer was found to be more permeabilized than the HRMEC-Vector monolayer in a cell permeability assay (Fig. 5c, mean fold change = 1.2 ± 0.19 , $p = 0.003$). This indicates that PRL3 overexpression in endothelial cells could compromise blood vessel integrity.

To dissect the impact of endothelial PRL3 overexpression on VEGF-related signaling mechanisms, western blotting of HRMEC-PRL3 and HRMEC-Vector was conducted. PRL3 overexpression enhanced the phosphorylation of ERK1/2 ($40.8\% \pm 18.8\%$ increase, $p = 0.02$) and paxillin ($49.8\% \pm 28.5\%$ increase, $p = 0.039$) but there was no apparent change in the expression of phosphorylated PLC γ 1 (Fig. 5f, g). Hence, PRL3 does not facilitate VEGF signaling via PLC γ 1. Increased phosphorylation of ERK1/2 and paxillin can result in enhanced endothelial proliferation and migration respectively^{54,55}. Interestingly, western blotting and immunofluorescence staining of HRMEC-PRL3 showed a reduction in the expression of ZO-1 (Fig. 5d, e, HRMEC-Vector: 9198.2 ± 526.9 versus HRMEC-PRL3: 7497.7 ± 1372.0 , $p = 0.032$), VE-Cadherin ($23\% \pm 6.2\%$ decrease, $p = 0.0028$), as well as increased phosphorylation of AKT ($68.5\% \pm 39.4\%$ increase, $p = 0.04$) and SRC ($39.6\% \pm 22.4\%$ increase, $p = 0.038$) (Fig. 5f, g). The downregulation of ZO-1 and VE-Cadherin could result in the weakening of the barrier function of HRMEC-PRL3 endothelial monolayer^{56,57}. Localisation of PRL3 is primarily at the cell membrane and cytoplasm of HRMEC-PRL3 (Fig. 5d, panel D). In addition, HRMEC-PRL3 have a lowered expression of VEGFR2 ($44.0\% \pm 5.1\%$ decrease, $p = 0.0001$) which might attenuate endothelial sensitivity to VEGF stimulation (Fig. 5f, g). Interestingly, HRMEC-PRL3 cells do not respond to the angiogenic inhibition of bevacizumab (up to a high dose of 10 mg/ml) to the similar extent as that for HRMEC-Vector cells (Supplementary Fig. 7). A schematic diagram (Fig. 5h) depicts the involvement of PRL3 in the VEGF signaling pathway under the endogenous and overexpression systems.

PRL3-zumab has a strong ocular and systemic safety profile

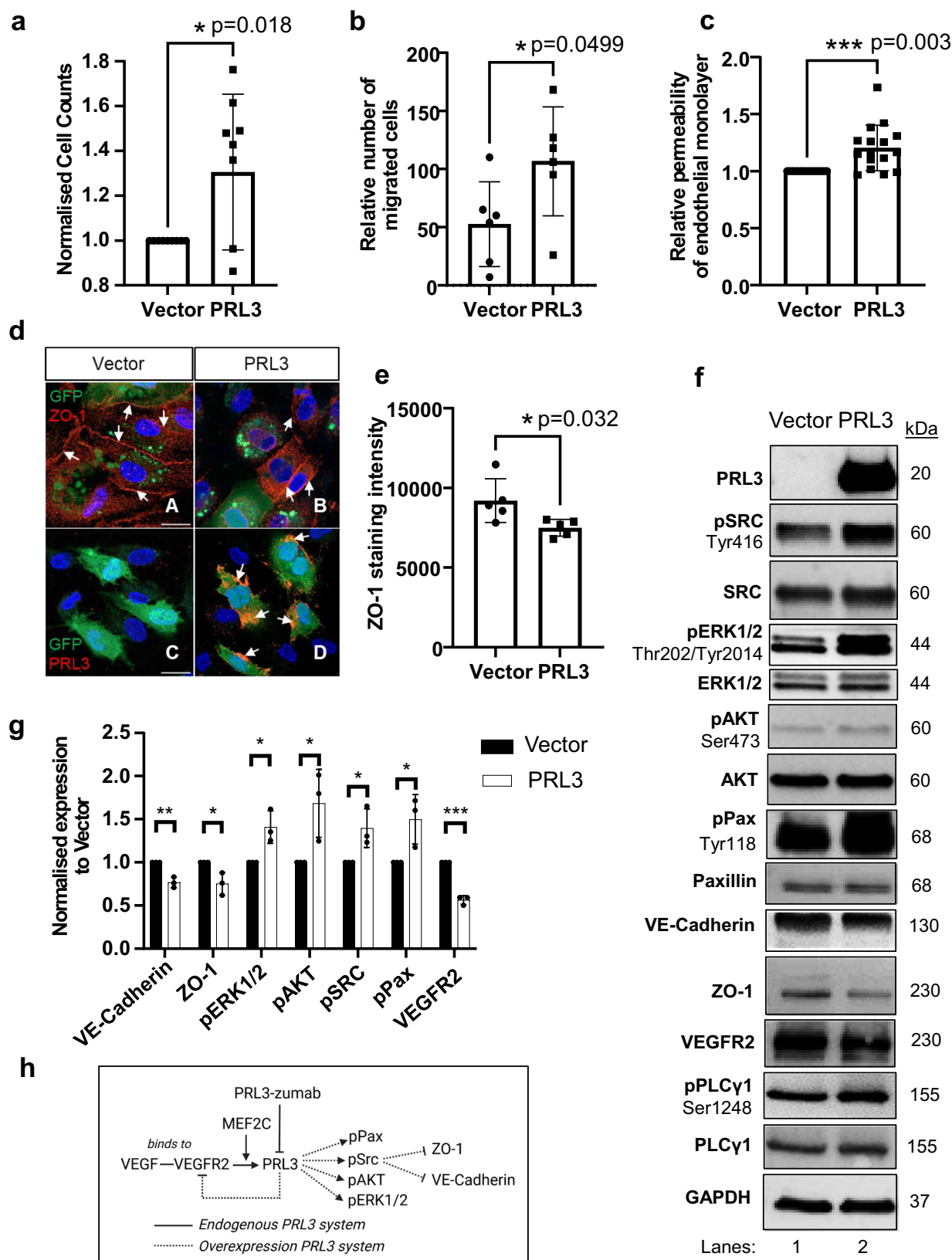
To investigate the safety profile of PRL3-zumab in human eyes, PRL3-zumab treatment on human ocular cell lines of retinal origin, namely HRMEC, ARPE-19 and M10-M1 Müller glial cells, was performed. We found that PRL3-zumab treatment was not cytotoxic to these ocular cell lines, even up to a high dose of 100 μ g/ml over 48 h (Fig. 6a–c). Toxicology studies of PRL3-zumab (IV) were done in 40 cynomolgus monkeys (20 males and 20 females) with biweekly intravenous bolus injection (up to 8 weeks, total of 5 doses) at doses of 0, 4, 12, and 36 mg/kg/day with an 8-week recovery period. This treatment schedule did not show drug-related ocular or overall systemic changes (Fig. 6d and Supplementary Table 1). Next, we performed toxicology

study of PRL3-zumab (IVT) in New Zealand White Rabbit model. PRL3-zumab was shown to bind to rabbit PRL3 protein (Supplementary Fig. 8). Toxicology study of PRL3-zumab (IVT) in New Zealand White Rabbit model did not show drug-related ocular toxicity. At all three doses of 0.084 mg, 0.175 mg and 0.35 mg, there was no significant change (pre- and post-dose) in intra-orbital pressure (Fig. 6e) and central corneal thickness (Fig. 6f). There was also no observed retinal abnormalities and no significant change in body weight for all 3 doses throughout the experiment (Supplementary Fig. 9). PRL3-zumab concentration in vitreous compartment after IVT antibody administration in non-injury induced rabbit model showed a two-fold reduction in vitreous antibody concentration from 8 hr timepoint to 144 hr timepoint (Supplementary Fig. 10), and the rate of elimination could be higher in a diseased condition. More importantly, PRL3-zumab (IV) has passed First-in-Man Phase I clinical trials in Singapore with a strong safety profile, without drug-related ocular and systemic severe adverse events (SAEs) or death³⁵. Collectively, we have strong evidence indicating that PRL3-zumab could potentially be safe for the human eyes. Hence, targeting PRL3 is a promising therapeutic option for neovascular eye diseases.

Discussion

Resistance to current anti-VEGF treatment regimens in patients suffering from nAMD and DR/DME is a challenge in the clinic. Beyond that, patients may have contraindications to different intravitreal injections, such as recent stroke or myocardial infarction for anti-VEGF therapies or a history of steroid response for intravitreal steroid injections. In recent years, there have been extensive efforts to discover new targets, as well as developing novel therapies like gene therapy and bispecific drugs that bind to a combination of pro-angiogenic molecules (including VEGF-A) to treat neovascular eye diseases⁵⁸. Most of these therapies are still in preclinical studies and clinical trials. In this study, we have identified PRL3 as a therapeutic target that is specifically upregulated in mouse models of nAMD and DR/DME and not in normal adult mouse ocular tissues. Thus, PRL3 serves as a useful therapeutic target for these diseases. Secondly, we demonstrated that anti-PRL3 antibody treatment significantly enhanced the recovery of CNV lesions with a strong safety profile. This is a proof-of-concept that PRL3-zumab could potentially be an alternative option for treating neovascular eye diseases. Thirdly, based on the disease-specific expression of PRL3, we have proposed delivering anti-PRL3 antibody via IV route instead of IVT to avoid IVT-associated risks of ocular side effects.

From literature, VEGF stimulation in endothelial cells leads to the upregulation of various signaling molecules such as pERK1/2, pAKT, pSRC, pPaxillin, and the downregulation of ZO-1 and VE-Cadherin^{54,55,57,59–61}. These changes result in the enhanced proliferation, migration, and permeability of the endothelial cell monolayer. Ultimately, this could lead to the abnormal growth of hyperpermeable blood vessels, which is the causative mechanism for neovascular eye diseases. In our study, we found that VEGF upregulates endogenous PRL3 protein in human retinal microvascular endothelial cells, which indicates that PRL3 is implicated in VEGF signaling. Interestingly, PRL3 overexpression alone, without VEGF stimulation, could promote retinal endothelial proliferation and migration via the phosphorylation of AKT, ERK1/2 and Paxillin^{54,55,59}. More importantly, PRL3 increases the permeability of the endothelial monolayer via SRC phosphorylation and downregulation of cell junctional proteins (ZO-1 and VE-Cadherin) which could promote vascular leakage^{57,60,61}. It is in line with published literature that described the inability of PRL3 knockout primary endothelial cells to phosphorylate SRC and paxillin in the presence of VEGF stimulation⁴³. PRL3 shares similar downstream effector signaling as VEGF. Due to the above-mentioned findings, PRL3 is likely to be one of the downstream drivers of proangiogenic signaling in neovascular eye diseases. Curiously, we also found that PRL3 overexpression in endothelial cells attenuates VEGFR2 expression which could be a



negative feedback loop under forced PRL3 overexpression that may drive some signaling events of VEGF and its receptors to trigger this feedback mechanism. Targeting PRL3 could thus be an alternative option for treating patients who suffer from neovascular eye diseases.

Interestingly, targeting intracellular PRL3 with an antibody demonstrates efficacy *in vivo*. This could be due to the permeabilizing

effect of VEGF on endothelial cell membranes, which allows access for antibody binding. Previous studies have demonstrated that VEGF increases the porosity of endothelial cells by increasing the number and size of pores of hepatic sinusoidal endothelial cells and has a permeabilizing effect^{62–64}. With regards to PRL3-zumab in cancer therapy, it has been reported that intracellular PRL3 protein was found

Fig. 5 | Endothelial PRL3 overexpression promotes HRMEC proliferation, migration and permeability by facilitating VEGF signaling. **a** HRMEC-PRL3 exhibits a higher rate of cell proliferation compared to HRMEC-Vector ($p = 0.018$, $n = 9$ replicates from three independent batches of transduced HRMECs). **b** HRMEC-PRL3 have a greater cell migratory ability compared to HRMEC-Vector ($p = 0.0499$, $n = 6$ replicates from three independent batches of transduced HRMECs). **c** There is an increased permeability in HRMEC-PRL3 monolayer compared to HRMEC-Vector ($p = 0.003$, $n = 16$ replicates from three independent batches of transduced HRMECs). **d** HRMEC-PRL3 monolayer have diminished ZO-1 cell surface expression compared to HRMEC-Vector by immunofluorescence staining. Both HRMEC-Vector and HRMEC-PRL3 have reporter GFP gene for successful retroviral infection of the plasmids. In the PRL3 panel (upper, panel B), there is a mixture of PRL3 overexpressing and wildtype cells, and stronger ZO-1 expression is seen in the wildtype cells (white arrows point to intact ZO-1 expression). In the PRL3 panel (lower, panel D), the white arrows point to the PRL3 localisation in the cell membrane and cytoplasm. Scale, 20 μm . **e** Quantification of ZO-1 staining intensity ($p = 0.032$, $n = 5$ from three independent batches of transduced HRMECs).

f Western blotting shows that HRMEC-PRL3 have increased levels in pERK1/2, pAKT, pSRC, pPaxillin and reduced expression of ZO-1, VE-Cadherin, and VEGFR2 compared to HRMEC-Vector. All data are representative images and western blots of three independent batches of transduced HRMECs for each experiment. **g** Quantification of Western blotting analysis (VE-Cadherin: $p = 0.0028$, ZO-1: $p = 0.03$, pERK1/2: $p = 0.02$, pAKT: $p = 0.04$, pSRC: $p = 0.038$, pPax: $p = 0.039$, VEGFR2: $p = 0.0001$). **h** Schematic model depicting the upregulation of endogenous PRL3 by VEGF via MEF2C, and PRL3's involvement in the downstream VEGF signaling in a forced overexpression system that promotes the phosphorylation of SRC, AKT, ERK1/2 and Paxillin, downregulation of ZO-1 and VE-Cadherin and a negative feedback loop resulting in a reduced VEGFR2 expression (Created in BioRender⁷³). Glyceraldehyde 3-phosphate dehydrogenase (GAPDH) served as loading control. All experiments were done using three independent batches of transduced HRMECs. The mean value was calculated by two-sided Student's *t*-test (mean \pm s.d., $n = 3$ replicates each). *** $P < 0.001$, ** $P < 0.01$, * $P < 0.05$. Source data are provided as a Source Data file.

to be externalized onto the surface of cancer cells due to the harsh conditions in the tumor microenvironment, that includes but not limited to hypoxia, nutrient deprivation, and necrosis. PRL3-zumab can then bind to externalized PRL3 and trigger host immune system in recruiting Natural Killer cells, B cells, and macrophages to kill cancer cells by antibody-dependent cellular cytotoxicity and antibody-dependent cellular phagocytosis (ADCC & ADCP) cascades²⁸.

In our study, we have demonstrated that IV administration of anti-PRL3 antibody has a superior efficacy compared to IVT drug delivery in the CNV mouse model due to a larger drug dose permitted by IV route. Vitreous antibody concentration is dependent on the molar concentration of antibody stock and volume of injected antibody. However, there are limitations to increasing the vitreous antibody concentration due to the limited increase in molar concentration of antibody stock and constraints in increasing injected antibody volume due to the small size of mouse eyes. IV delivery could overcome the limitations of IVT delivery. On Day 7 (6 days post IVT), the anti-PRL3 antibody concentration in the serum was comparatively higher (1185.1 ± 25.8 ng/mL) than that of the vitreous compartment (13.6 ± 1.7 ng/mL), indicating that most of the drug had entered systemic circulation. However, via IV administration, the vitreous drug concentration remained relatively high (69.8 ± 11.1 ng/mL, $\sim 5\times$ greater than that of IVT) and the corresponding serum drug concentration was considerably high (21159.0 ± 2472.1 ng/mL) at Day 7. This difference in efficacy could be that the antibody delivered by IV had a longer half-life ($T_{1/2}$) in the serum with sustained antibody levels in the vitreous compartment for a longer duration due to the state of equilibrium compared to that of IVT.

However, IV drug administration has its limitations. First, the drug candidate will have to be safe as IV delivery causes systemic circulation of the drug, and this could increase the risk of side effects. Second, IV drug administration will require a larger amount of the drug, which could increase the cost of treatment. Prior to the advent of anti-VEGF therapies, Verteporfin – an intravenously injected drug – was used in conjunction with laser in photodynamic therapy to treat abnormal growth of hyperpermeable blood vessels in nAMD^{65,66}, and is currently used in the management of polypoidal choroidal vasculopathy⁶⁷. Additionally, systemic administration of anti-VEGF drugs (bevacizumab and aflibercept) has been reported to demonstrate promising efficacy in nAMD patients, but the concerns of drug-related adverse events led to the discontinuity of exploring into this route of drug administration^{68–70}. Consequently, current anti-angiogenic therapy used in nAMD and DR/DME is only administered via the IVT route. Our proposed treatment is the first clinically safe anti-angiogenic therapy by IV administration that could be used to treat neovascular eye diseases. To date, PRL3-zumab, via IV, has passed Phase I clinical trials in Singapore with an excellent safety profile³⁵. Hence, it is safe to

use PRL3-zumab by IV delivery to treat neovascular eye diseases. Moving forward, there is a need to perform dose titration of PRL3-zumab in human subjects to ensure a balance of safety, efficacy and cost for patients.

The discovery of PRL3 as a therapeutic target in neovascular eye diseases presents an alternative solution to the management of these diseases. It is plausible that PRL3-zumab could be repurposed to treat neovascular eye diseases in the near future.

Methods

Ethical statement

Our research complies with all relevant ethical regulations. The collection and use of human tumor sections were approved by A*STAR Institutional Review Board (2019-039). All mice used in the studies were handled according to the protocols (#232751, #221735) approved by the Institutional Animal Care and Use Committee (IACUC) of A*STAR (Singapore), and protocol (2020/SHS/1597) approved by IACUC of Singapore Eye Research Institute (SERI). Rabbit and monkey toxicology experiments were conducted according to the protocols approved by the IACUC of Singapore Eye Research Institute (SERI) and Wuxi Apptec.

Whole mount mouse embryo staining

E9.5 embryos were fixed in 2% paraformaldehyde for 30 minutes and washed with washing buffer (0.1% Triton-PBS). The fixed embryos were then immersed in an ascending concentration of methanol from 50% to 75% and to 100% for 20 minutes each. After which, the embryos were incubated in 1%–2% of H_2O_2 in methanol for 45 minutes and then immersed in descending concentration of methanol from 75% to 50% and to 25% for 20 minutes each. These embryos were then washed twice with 0.1% Triton-PBS and subsequently blocked with blocking buffer (2% Skim milk + 0.2% Triton-X in PBS) for 2 hours at 4 °C. These were then incubated in primary antibodies diluted in blocking buffer (CD31, 1:200; Ter119, 1:200; vWF, 1:200; PRL3, 1:200) overnight at 4 °C. The next day, these were washed with washing buffer thrice for 10 minutes each and then incubated with respective secondary antibodies (1:1000) for 3 hours at room temperature. After which, these were washed with washing buffer thrice, once with PBS and once with 1XTBS for 10 minutes each. Finally, the embryos were incubated with DAB (7.5 mg DAB + 2 μl H_2O_2 + 15 ml TBS) for 5 minutes until brown coloration appeared and washed thrice with PBS. The stained samples were then ready for imaging.

Laser-induced choroidal neovascularization (CNV) mouse model

The CNV mouse model is adopted to recapitulate neovascular AMD in humans. In the laser-induced CNV mouse model, eight-week-old C57BL6/J male mice were used. The mice were housed with access to

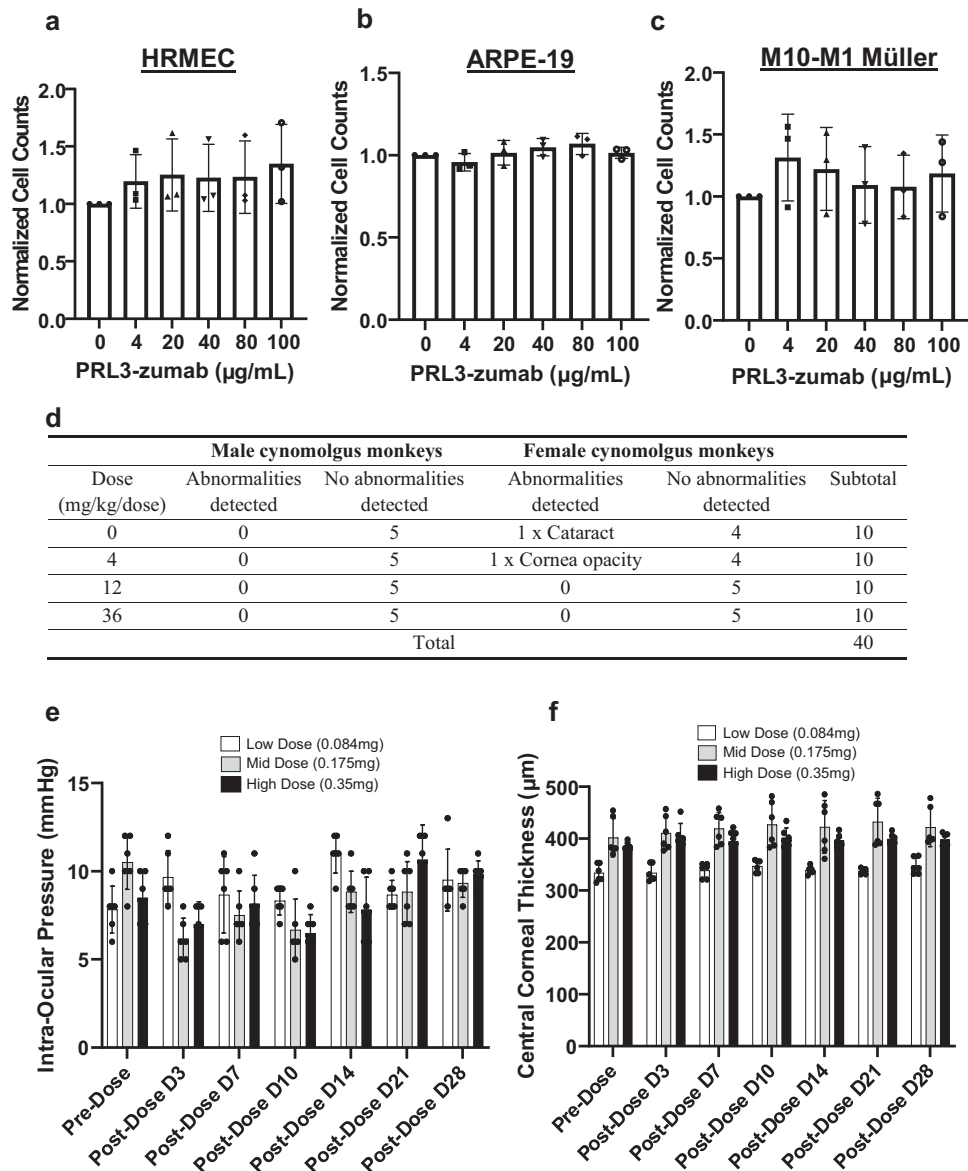


Fig. 6 | PRL3-zumab is non-toxic to the ocular compartment. **a–c** There was no observed cytotoxicity of PRL3-zumab on human ocular cell lines (**a**, HRMECs; **b**, ARPE-19; **c**, M10-M1 Müller glial) up to 100 µg/mL of PRL3-zumab for 48 h. The experiments were conducted thrice (3 technical replicates each), and the data are mean ± s.d. for each group. **d** Summary of ophthalmological-related toxicology results of intravenous administration of PRL3-zumab in cynomolgus monkeys. This toxicology study involved biweekly intravenous bolus injection of PRL3-zumab (total 5 doses) in 40 cynomolgus monkeys (20 males and 20 females) followed by an 8-week recovery period. In this study, there were ocular abnormalities in 2 individual female cynomolgus monkeys, that is, one with cataract at 0 mg/kg/dose

and the other with cornea opacity at 4 mg/kg/dose. However, it was not observed in the male counterparts at higher doses. There was no observed ocular toxicity related to intravenous administration of PRL3-zumab up to a high dose of 36 mg/kg/dose in Cynomolgus monkeys. **e, f** Toxicology studies of intravitreal administration of PRL3-zumab in New Zealand White Rabbits demonstrated no significant change in intraocular pressure and central corneal thickness ($n = 6$ eyes, 3 rabbits in each group). The data are presented as mean ± s.d. HRMEC: Human Retinal Microvascular Endothelial Cells; ARPE-19: Human Retinal Pigment Epithelial Cells; M10-M1 Müller: Human glial cells. Source data are provided as a Source Data file.

standard mouse chow and water in a specific pathogen-free mouse facility of the Biological Resource Centre with controlled temperature and humidity. The mice were anesthetized using a combination of ketamine (150 mg/kg body weight) and xylazine (10 mg/kg body weight) and pupils dilated using a topical administration of 1 drop of 1% tropicamide (Alcon Laboratories, Inc., Fort Worth, TX, USA) and 1 drop of 1% phenylephrine (Bausch and Lomb Pharmaceuticals, Inc., Tampa, FL, USA) ophthalmic solutions. Laser induction was done using the MICRON IV retinal imaging system (50 µm spot size, 0.05 second duration, 150 mW) in the posterior pole of the retina. 4 spots were given to each eye. One week after laser burn, mice were sacrificed in a CO₂ euthanasia chamber. The neural retina and retinal pigment

epithelium-choroid complex (RPE-choroid) were then harvested for western blotting. Euthanasia of mice was humanely executed using CO₂ inhalation according to the institutional guidelines and ethical regulations.

Drug treatment was given by intravitreal (IVT) or intravenous (IV) routes. For IVT, a standard-of-care dose of 2.5 µg of drug (Eylea or mouse anti-PRL3 antibody) was carefully injected under the dissection microscope. It was administered on day 1 after FFA and OCT images were taken. Once-off IVT injection follows the clinical regimen of one dose/month. For IV, 100 µg of drug (mouse anti-PRL3 antibody) was administered by tail vein injection on day 1 and day 4. PBS/mouse IgG were used as a negative control. Twice weekly IV injection regimen

(100 µg, 5 mg/kg) is the treatment regimen that we have adopted in anti-PRL3 antibody in mouse cancer studies, which have demonstrated significant tumor reduction³². This regimen shows effective target engagement of anti-PRL3 antibody and serves as an important reference for the CNV experiment. Animal experiments were strictly adhered to approved protocols (#232751 and #221735).

Oxygen-Induced Retinopathy (OIR) mouse model

The OIR mouse model is adopted to mimic some aspects of DR/DME in humans. OIR was conducted as described⁴⁸. The mice were housed with access to standard mouse chow and water in a specific pathogen-free mouse facility of SingHealth Experimental Medicine Centre (SEMC), Translational Pre-Clinical Model Research Platform with controlled temperature and humidity. In short, nursing mums and post-natal day 7 (P7) pups (mixed gender) were housed in a 75% oxygen chamber for 5 days and then in room air subsequently for 5 days. After which, the pups were sacrificed in a CO₂ euthanasia chamber, and the neural retina and retinal pigment epithelium-choroid complex (RPE-choroid) were harvested for western blotting analyses. Euthanasia of pups was humanely executed using CO₂ inhalation according to the institutional guidelines and ethical regulations. Animal experiments were strictly adhered to approved protocols (#2020/SHS/1597).

Fundus fluorescein angiography (FFA)

Digital color fundus images were taken using a MICRON IV comprehensive system for rodent retinal imaging (Phoenix Research Laboratories, Pleasanton, CA, USA). Mice were anesthetized and pupils were dilated as described above. After dilation, both eyes of the mice will be covered with a layer of viscid gel to aid in ocular imaging and also to prevent drying of the cornea during the procedure. The whole procedure took about 15–20 minutes per mouse in a dim room. Mice were immediately placed near a red heat lamp after the procedure to maintain body temperature. Digital colored retinal photographs were captured from the mice during pupil dilation. For FFA, mice were given, via intraperitoneal injection, 10% sodium fluorescein dye at a dose of 0.01 mL per 5 to 6 g body weight and fundus images were taken using MICRON IV. FFA was performed 24 hours and 6 days post laser induction, and these were set as Day 1 baseline and Day 6 measurements. The images were then analysed using Fiji-ImageJ (1.53c) software, in which the vascular leakage area was marked out and measured by excluding the value of large vessels (with gray value more than 100). Using spot-to-spot comparison, the vascular leakage area of each spot in day 7 images was compared against the same spot in Day 1 images. The difference between the two measurements was expressed as a percentage of healing. The numbers of CNV spots in the treatment groups used in analysis are as follow: IVT - PBS/IgG (*n* = 34), anti-PRL3 ab (*n* = 53), aflibercept (*n* = 21); IV - PBS/IgG (*n* = 25), anti-PRL3 ab (*n* = 48).

Image-guided optical coherence (OCT) tomography

To perform OCT, mice were anaesthetized and their eyes dilated (as described above). An OCT module + objective lens is attached to the MICRON IV imaging system. Using a live colored fundus image as a guide, a stacked image is generated for multiple retina layers.

Immunohistochemistry

The collection and use of human tumor sections were approved by A*STAR Institutional Review Board (2019-039). The tumors were identified as PRL3+ or PRL3- by Western blotting with a band at 20 kDa or by IHC with mouse anti-PRL3 antibody for positive staining. Samples were blocked with blocking buffer (2% BSA, 5% FBS, and 5% goat serum in 1xPBS) for an hour. After which, primary antibody incubation was done overnight at 4 °C. Primary antibodies: CD31 (GeneTex JC/70 A, GTX73514, 1:25) and αSMA (ThermoFisher, A700-082, 1:250). Stained samples were washed with PBS-T (1xPBS with 0.2% Tween-20) thrice

for 5 minutes each. These samples were then incubated with fluorophore-conjugated secondary antibodies (ThermoFisher, Alexa Fluor 488 and 568) for 2 hours in the dark and subsequently washed thrice with PBS-T. Next, samples were stained with DAPI (1 µg/mL) for 20 minutes and washed twice with 1xPBS. Finally, coverslips were mounted using mounting medium (Vectorlab, H-1000) and were ready to be imaged using confocal microscopy (Zeiss). At least 5–10 10X images were taken from each tumor section.

Quantification of pericyte coverage

Using the images of CD31 and αSMA-stained tumor sections, pericyte coverage of each image was calculated by dividing total CD31⁺αSMA⁺ (double positive) counts by CD31⁺ (single positive) counts, multiplied by 100. The mean was then computed and represented as for the entire tumor section.

Cell culture

Human Retinal Microvascular Endothelial Cells (HRMECs) (angio-proteomie (cAP-0010)) were cultured on flasks coated with Quick Coating Solution (angio-proteomie (cAP-01)), in Endothelial Growth Medium (LONZA (CC-3162)). ARPE-19 (ATCC, CRL-2302) and MIO-M1 Müller glial cells (RRID:CVCL_0433) were cultured in Dulbecco's Modified Eagle Medium (Gibco) supplemented with 10% (v/v) fetal bovine serum (Hyclone) and 1% (v/v) Penicillin-streptomycin (ThermoFisher).

SDS-PAGE and western blotting

Mouse tissues were homogenized in RIPA buffer with phosphatase inhibitors and protease inhibitors (Roche). Protein concentration was quantified using BCA dye and spectrophotometer at an absorbance 450 nm. 70 µg of protein per sample was loaded, and 15% Tris-tricine gel was run for PRL3 detection, and 8% Tris-glycine gel for the detection of other markers. Primary antibodies: mouse PRL3 antibody (318) (in-house, 1:1000), humanized PRL3 antibody (PRL3-zumab, 1:1000), phospho-SRC (CST6943, 1:1000), SRC (CST2109, 1:1000), phospho-ERK1/2 (CST4370, 1:2000), ERK1/2 (CST4695, 1:1000), phospho-paxillin (CST2541, 1:1000), paxillin (CST2542, 1:1000), phospho-AKT (CST4060, 1:2000), AKT (CST4691, 1:1000), VEGFR2 (ab39638, 1:500), ZO-1 (ThermoFisher Scientific 33-9100, 1:1000), VE-Cadherin (ab205336, 1:1000), phospho-PLCγ1 (CST8713, 1:1000), PLCγ1 (CST5690, 1:1000), GAPDH (Sigma CB1001, 1:3000), β-Actin (CST 4970S, 1:1000), HRP- rabbit anti-mouse secondary antibody (Jackson ImmunoResearch, 315-035-046, 1:1000), HRP- donkey anti-human secondary antibody (Jackson ImmunoResearch, 709-035-098, 1:1000), HRP- goat anti-mouse secondary antibody (ThermoFisher, 31432, 1:1000), HRP-linked anti-rabbit secondary antibody (CST 7074S, 1:1000).

MEF2C silencing and inhibition experiments

For *MEF2C* silencing, either 200 pM of a non-targeting Stealth RNAi negative control (Life technologies, cat. #12935300), or *MEF2C*-specific siRNA (HSS181064, Life technologies, cat. #1299001 - Sense: 5'-CAGC GCUCUACCCUUGGUUCAGUA-3'; Anti-sense: 5'-UACUGAACCAAGG UGAAGAGCGCUG-3') was transfected into HRMECs using lipofectamine RNAiMAX Reagent (Invitrogen, cat. #13778). For *MEF2C* inhibition, cells were treated with 0.1 mg/ml Pamapimod (MedChemExpress LLC, cat. # HY-10405).

qPCR analysis

RNA was extracted using RNeasy mini kit (QIAGEN, cat. #74104) and reverse transcribed using the High-Capacity cDNA Reverse Transcription kit (Applied Biosystems, cat. #4368814). qPCR was conducted with SyBr green (Biorad, iTaq Universal SyBr green Supermix, cat. #1725121) using the RTPCR system (Biorad, CFX96 Real-time system). Samples were normalized to β-actin. The experiments were conducted according to the manufacturer's instructions.

Primers used in this study are: PRL3 - Forward: 5'-CAAACA-CATGCGCTTCCTCA-3'; Reverse: 5'-AGCGGCGTTTGTGTCATAGGT-3'. MEFC2 - Forward: 5'-TTCCAGTATGCCAGCACCG-3'; Reverse: 5'-GGCCCTTCTTTCTCAACGTCTC-3'. β -actin - Forward: 5'-GCTCACCATTGGATGATGATATCGC-3'; Reverse: 5'-ATAGGAATCCTTCTGACCCATGCC-3'.

Immunofluorescence

A total of 1×10^4 of HRMECs (Vector, PRL3) were seeded onto glass coverslips in 12-well culture plate. Cells were subsequently fixed in 2.7% PFA for 15 minutes, washed in PBS-Tween (0.1%), permeabilized with PBS-Triton (0.1%), and blocked with 2% BSA + 5% Goat serum + 5% FBS in PBS (blocking buffer) for an hour. Primary antibodies were diluted in blocking buffer and added onto the cells and incubated at 4 °C overnight. Primary antibodies: ZO-1 (ThermoFisher Scientific 33-9100, 5 μ g/ml), mouse PRL3 (in-house, 1:100). These stained cells were then incubated with fluorophore-conjugated secondary antibodies (ThermoFisher, Alexa fluor 568) for 2 hours in the dark and subsequently washed thrice with PBS-Tween (0.1%). Subsequently, the samples were stained with DAPI (1 μ g/mL) for 10 minutes and washed twice with 1xPBS. Finally, the coverslips with stained cells were mounted onto glass slides using mounting medium (Vectorlab, H-1000) and were ready to be imaged using confocal microscopy (Zeiss).

Quantification of anti-PRL3 antibody concentration in mouse serum and vitreous humor samples

Serum samples were collected at pre dose, 24 and 72 hours after IVT and at the end of the experiment. Vitreous samples were collected at the end of experiment. Anti-PRL3 antibody concentration in serum and vitreous were analyzed by ELISA method. Briefly, 96-well plates coated overnight with GST-PRL3 (1ng) were blocked with 3% bovine serum albumin in PBS-0.05% Tween-20 prior to incubation with serum sample (1:20000) for 1 h at 37 °C. After extensive washing, HRP-conjugated anti-mouse antibody (Jackson) was added for 1 h at 37 °C. Colorimetric development was performed using a Turbo-TMB substrate (Pierce) and stopped by acidification with 2 M H_2SO_4 . Absorbance was measured at 450 nm using a plate reader (Tecan).

VEGF treatment of HRMECs

2×10^5 HRMECs were seeded in a well of a 6-well plate. After the cells have attached overnight, the cells were starved with endothelial basal medium (LONZA) for 3 h at 37 °C in a 5% CO_2 atmosphere. Recombinant human VEGF protein (RnD Systems) was then added in the media to make up the final concentration of 50 ng/ml. The cells were harvested 24 h, 48 h and 72 h after VEGF treatment for protein analysis.

Retroviral infection of HRMECs

To establish HRMEC cells overexpressing PRL3 (HRMEC-PRL3) and a control cell line (HRMEC-Vector), HRMEC-WT cells were transduced with retrovirus that were made by transfecting Human Embryonic Kidney 293 T (HEK293T) cells along with the packaging vector. The pEGFP-C1-PRL3 construct has been described previously⁴¹. PRL3 cDNA was amplified from pEGFP C1-PRL3 plasmid and cloned into the retroviral vector. The conditioned media (with the retrovirus) was concentrated, aliquoted and stored at -80 °C until usage. The virus was then titrated in Endothelial Growth Media-2 (EGM2) and added to HRMECs. The successful transduction could be observed by the GFP signal. HRMECs were harvested and PRL3 overexpression was confirmed by Western blotting.

CRISPR Knockout of PRL3 in HRMECs

LentiCRISPRv2 (Addgene, #52961) was the backbone for sgRNAs used in the CRISPR/Cas9 knockout experiments. For cloning, plasmid was digested using **BsmBI** and gel extracted (Qiagen, cat. #28704).

Oligonucleotides were annealed and ligation reaction was performed using T4 DNA ligase (NEB, cat. #M0202) at 16 °C overnight. Plasmids were heat shock transformed into chemically competent *E. coli* bacteria (ThermoFisher Scientific, One Shot TOP10, cat. #C404003) and minipreps were performed (Qiagen, cat. #27115).

Sequences of sgRNA oligos are: sgRNA #2: Forward - 5'-CACC GTCTTCCACTACCTTGCCGGG-3', Reverse - 5'-AAACCCCGCAAGG-TAGTGAAGAC-3'; sgRNA #3: Forward - 5'-CACCGTGGCGCGC GCCTACCACAA-3', Reverse - 5'-AAACTTGTGGTGAGGCGCGCGC-CAC-3'. Lentiviruses were produced by transfecting HEK293T cells with jet-PEI (polypus, #101-10 N) in combination with helper plasmids PMDLg/pRRE, pMD2.G and pRSV-Rev at a ratio of 2:1:1. The conditioned media (with the lentivirus) was titrated in EGM2 and added to HRMECs. The cells were cultured further for two weeks before the cells were harvested and PRL3 knockout was confirmed by Western blotting and qPCR analyses.

Drug treatment in HRMECs

A total of 5×10^5 HRMECs were seeded in 10-cm dishes and cultured in an incubator (37 °C, 5% CO_2). Cells were stimulated with VEGF (50 ng/ml) for 2 days before PRL3-zumab (100 μ g/ml, IISG) treatment or bevacizumab (10 mg/ml, Amgen, MVASI, cat. #1026700) treatment for further 2 days. At the end of the experiment, treated cells were pelleted and harvested for protein analysis.

Cell proliferation assay

The proliferation rates of HRMECs (HRMEC-WT, HRMEC-PRL3) were evaluated using the MTS (3-(4,5-dimethylthiazol-2-yl)-5-(3-carboxymethoxyphenyl)-2-(4-sulfophenyl)-2H-tetrazolium)-based CellTiter 96 Aqueous One Solution Cell Proliferation Assay (Promega). This experiment was conducted in accordance with the manufacturer's protocol. 2×10^3 cells were seeded in complete media (EGM2) into each well of a 96-well plate and allowed to attach overnight. The cells were seeded in triplicates. The media was subsequently changed with complete media containing PBS or PRL3-zumab (4, 20, 40, 80, 100 μ g/ml) and the cells were then incubated for 48 h at 37 °C in 5% CO_2 atmosphere. After which, the media was aspirated and 100 μ L fresh media containing MTS (Promega) was then added, and formazan development was done for 2 h at 37 °C and 5% CO_2 before absorbance at 490 nm was read using a spectrophotometer (Tecan).

Cell migration assay

2×10^3 cells (HRMEC-WT, HRMEC-PRL3) were seeded in the upper chamber of the transwell plate (Corning #3422) in 200 μ L of serum-free EBM2 with 500 μ L of EGM2 (with FBS) in the lower chamber as chemoattractant. Cells were incubated for 24 h at 37 °C and 5% CO_2 . After which, non-migrating cells on the upper chamber were scraped off with a cotton swab. Migrated cells (at the bottom of the membrane) were stained with 0.1% crystal violet for 30 minutes. Thereafter, the membrane was washed with distilled water for 30 seconds to remove residual dye and then air dried overnight. Images were taken at X20 magnification, and cells were counted.

Endothelial cell monolayer permeability assay

Using the endothelial 24-well transwell permeability assay kit (Cell Biologics, CB6929), 5×10^3 cells (HRMEC-WT, HRMEC-PRL3) were seeded on the 6.5 mm transwell insert membrane in 200 μ L of EGM2. 1 mL of EGM2 was added in the experimental wells. The transwell inserts were transferred using a sterilized forceps to the wells containing 1 mL EGM2 and incubated for 4 days at 37 °C and 5% CO_2 until the cells grew to 100% confluence. Cells were starved with EBM2 for 3 h, and 300 μ L of fresh EBM2 (including 5 μ L of streptavidin-HRP) was added to the top insert chamber of each well. 1 mL of EBM2 was added into the wells of a new 24-well plate and the inserts were transferred to the wells and incubated at 37 °C and 5% CO_2 for 24 h. 20 μ L of media

was transferred from the lower chamber to the wells of 96-well plate. Each sample would be aliquoted in triplicates. Finally, 50 μ L of TMB substrate was added into each well and incubated in a shaker for 2 minutes until the blue coloration appeared and the reaction was terminated by adding 50 μ L of stop solution at which it turned yellow. Absorbance reading at 450 nm was recorded in a spectrophotometer (Tecan).

Toxicology study of PRL3-zumab (IV) in Cynomolgus Monkeys

The study involved biweekly intravenous bolus injection of PRL3-zumab in 40 cynomolgus monkeys at 4 different dose levels (0, 4, 12, 36 mg/kg/dose) with 5 males and 5 females in each level, followed by an 8-week of recovery period. Eyes were examined once at predose for all animals and once during the last week of the dosing period. Prior to the examination, a mydriatic containing 1.0% Tropicamide was administered to dilate the pupils. All animals were examined via slit lamp and indirect ophthalmoscope. Other non-ophthalmological tests were conducted that included infusion reaction, body weight, organ weight, body temperature, ECG (electrocardiogram) reading, blood pressure, heart rate, respiratory system, neurological system, necropsy test, histopathology, serum chemistry, hematology tests, coagulation, urinalysis, and monitoring of bowel movements. This study was performed by Wuxi Aptec.

Toxicology study of PRL3-zumab (IVT) in New Zealand White Rabbits

This study involves one dose of PRL3-zumab via intravitreal delivery in a total of 9 rabbits at 3 dose levels (0.84 mg, 0.175 mg, 0.35 mg per 35 μ L). All animals were examined using slit lamp, fundoscope and pachymetry. This study was conducted by Singapore Eye Research Institute (SERI).

Statistical analysis

Data are represented as means S.D. Statistical analyses were performed by two-sided *Student's t* test and One-way Analysis of Variance ANOVA (Kruskal-Wallis) using Prism 10.4.1 (GraphPAD Software Inc.). *P* values of <0.05 (*), <0.01 (**), <0.001 (***) and <0.0001 (****). Each represents significant statistical comparisons among the listed experimental groups.

Reporting summary

Further information on research design is available in the Nature Portfolio Reporting Summary linked to this article.

Data availability

Data supporting the findings of this study are available in the article, its Supplementary information and the Source Data file. Additional information is available from the corresponding authors upon request. Source data are provided with this paper.

References

- World report on vision. Geneva: World Health Organization; 2019. Licence: CC BY-NC-SA 3.0 IGO.
- Miller, J. W. et al. Vascular endothelial growth factor/vascular permeability factor is temporally and spatially correlated with ocular angiogenesis in a primate model. *Am. J. Pathol.* **145**, 574–584 (1994).
- Adamis, A. P. et al. Increased vascular endothelial growth factor levels in the vitreous of eyes with proliferative diabetic retinopathy. *Am. J. Ophthalmol.* **118**, 445–450 (1994).
- Yuzawa, M. Treatment of exudative age-related macular degeneration. *Nippon Ganka Gakkai Zasshi* **104**, 875–898 (2000).
- van Lookeren Campagne, M., LeCouter, J., Yaspan, B. L. & Ye, W. Mechanisms of age-related macular degeneration and therapeutic opportunities. *J. Pathol.* **232**, 151–164 (2014).
- Romero-Aroca, P. et al. Diabetic macular edema pathophysiology: Vasogenic versus Inflammatory. *J. Diab. Res.* **2016**, 2156273 (2016).
- Wang, X. & Ohji, M. Vascular endothelial growth factor and its inhibitor in age-related macular degeneration. *Taiwan J. Ophthalmol.* **3**, 128–133 (2013).
- Blinder, K. J. et al. Anti-VEGF treatment of diabetic macular edema in clinical practice: effectiveness and patterns of use (ECHO Study Report 1). *Clin. Ophthalmol. (Auckl., N. Z.)* **11**, 393–401 (2017).
- Kwong, T. Q. & Mohamed, M. Anti-vascular endothelial growth factor therapies in ophthalmology: current use, controversies and the future. *Br. J. Clin. Pharm.* **78**, 699–706 (2014).
- Pożarowska, D. & Pożarowski, P. The era of anti-vascular endothelial growth factor (VEGF) drugs in ophthalmology. *VEGF anti-VEGF Ther. Cent. Eur. J. ofnbs;Immunol.* **41**, 311–316 (2016).
- Liberski, S., Wichrowska, M. & Kocięcki, J. Aflibercept versus faricimab in the treatment of neovascular age-related macular degeneration and diabetic macular edema: A review. *Int. J. Mol. Sci.* **23**, 9424 (2022).
- Osaadon, P., Fagan, X. J., Lifshitz, T. & Levy, J. A review of anti-VEGF agents for proliferative diabetic retinopathy. *Eye* **28**, 510–520 (2014).
- Villegas, V. M., Aranguren, L. A., Kovach, J. L., Schwartz, S. G. & Flynn, H. W. Current advances in the treatment of neovascular age-related macular degeneration. *Expert Opin. Drug Deliv.* **14**, 273–282 (2017).
- Yang, S., Zhao, J. & Sun, X. Resistance to anti-VEGF therapy in neovascular age-related macular degeneration: a comprehensive review. *Drug Des., Dev. Ther.* **10**, 1857–1867 (2016).
- Arima, M. et al. Claudin-5 redistribution induced by inflammation leads to anti-VEGF-resistant diabetic macular edema. *Diabetes* **69**, 981 (2020).
- Nesmith, B. L. W., Ihnen, M. & Schaal, S. Poor responders to bevacizumab pharmacotherapy in age-related macular degeneration and in diabetic macular edema demonstrate increased risk for obstructive sleep apnea. *RETINA* **34**, 2423–2430 (2014).
- Mettu, P. S., Allingham, M. J. & Cousins, S. W. Incomplete response to Anti-VEGF therapy in neovascular AMD: Exploring disease mechanisms and therapeutic opportunities. *Prog. Retinal Eye Res.* **82**, 100906 (2021).
- Rob, J. V. G. et al. A shift in the balance of vascular endothelial growth factor and connective tissue growth factor by bevacizumab causes the angiofibrotic switch in proliferative diabetic retinopathy. *Br. J. Ophthalmol.* **96**, 587 (2012).
- Kuiper, E. J. et al. The angio-fibrotic switch of VEGF and CTGF in proliferative diabetic retinopathy. *PLOS ONE* **3**, e2675 (2008).
- Neves, K. B., Montezano, A. C., Lang, N. N. & Touyz, R. M. Vascular toxicity associated with anti-angiogenic drugs. *Clin. Sci.* **134**, 2503–2520 (2020).
- Rosenstein, J. M., Krum, J. M. & Ruhrberg, C. VEGF in the nervous system. *Organogenesis* **6**, 107–114 (2010).
- Vazquez-Alfageme, C., Nicholson, L., Hamilton, R. D. & Patel, P. J. Incidence and long-term visual acuity outcomes of retinal pigment epithelium tears after intravitreal anti-vascular endothelial growth factor treatment for neovascular age-related macular degeneration. *Retina* **39**, 664–669 (2019).
- Lechner, J. et al. Alterations in circulating immune cells in neovascular age-related macular degeneration. *Sci. Rep.* **5**, 16754 (2015).
- Lin, J. B. et al. Targeting cell-type-specific, choroid-peripheral immune signaling to treat age-related macular degeneration. *Cell Rep. Med.* **5**, 101353 (2024).
- Espinosa-Heidmann, D. G. et al. Macrophage depletion diminishes lesion size and severity in experimental choroidal neovascularization. *Invest Ophthalmol. Vis. Sci.* **44**, 3586–3592 (2003).
- Hellenthal, K. E. M., Brabenec, L. & Wagner, N. M. Regulation and dysregulation of endothelial permeability during systemic inflammation. *Cells* **11**, 1935 (2022).

27. Al-Aidaroos, A. Q. O. & Zeng, Q. PRL-3 phosphatase and cancer metastasis. *J. Cell. Biochem.* **111**, 1087–1098 (2010).
28. Thura, M. et al. PRL3-zumab as an immunotherapy to inhibit tumors expressing PRL3 oncoprotein. *Nat. Commun.* **10**, 2484 (2019).
29. Chia, P. L., Ang, K. H., Thura, M. & Zeng, Q. PRL3 as a therapeutic target for novel cancer immunotherapy in multiple cancer types. *Theranostics* **13**, 1876–1891 (2023).
30. Li, J. et al. Generation of PRL-3- and PRL-1-specific monoclonal antibodies as potential diagnostic markers for cancer metastases. *Clin. Cancer Res.* **11**, 2195 (2005).
31. Guo, K., Tang, J. P., Tan, C. P., Wang, H. & Zeng, Q. Monoclonal antibodies target intracellular PRL phosphatases to inhibit cancer metastases in mice. *Cancer Biol. Ther.* **7**, 750–757 (2008).
32. Guo, K. et al. Targeting intracellular oncoproteins with antibody therapy or vaccination. *Sci. Transl. Med.* **3**, 99ra85 (2011).
33. Thura, M. et al. PRL3-zumab, a first-in-class humanized antibody for cancer therapy. *JCI Insight* **1**, e87607 (2016).
34. Thura, M. et al. PRL3 induces polypoid giant cancer cells eliminated by PRL3-zumab to reduce tumor relapse. *Commun. Biol.* **4**, 923 (2021).
35. Chee, C. E. et al. A Phase I, First-in-Human Study of PRL3-zumab in Advanced, Refractory solid tumors and hematological malignancies. *Target. oncol.* **18**, 391–402 (2023).
36. NCT04118114. Phase II Study of PRL3-ZUMAB in advanced solid tumors. Vol. 2024 (ClinicalTrials.gov, ClinicalTrials.gov, 2024).
37. NCT04452955. A study to assess safety and efficacy of PRL3-zumab in patients with solid tumors. Vol. 2024 (ClinicalTrials.gov, 2024).
38. CTR20211180. 一项针对实体瘤、评估PRL3-Zumab安全性和有效性的开放标签、多中心2期研究. Vol. 2024 (Chinadrugtrials, 2024).
39. Guo, K. et al. Catalytic domain of PRL-3 plays an essential role in tumor metastasis: formation of PRL-3 tumors inside the blood vessels. *Cancer Biol. Ther.* **3**, 945–951 (2004).
40. Parker, B. S. et al. Alterations in vascular gene expression in invasive breast carcinoma. *Cancer Res.* **64**, 7857–7866 (2004).
41. Guo, K. et al. PRL-3 initiates tumor angiogenesis by recruiting endothelial cells in vitro and in vivo. *Cancer Res* **66**, 9625–9635 (2006).
42. Xu, J. et al. VEGF promotes the transcription of the human PRL-3 gene in HUVEC through transcription factor MEF2C. *PLoS one* **6**, e27165–e27165 (2011).
43. Zimmerman, M. W. et al. Protein-tyrosine phosphatase 4A3 (PTP4A3) promotes vascular endothelial growth factor signaling and enables endothelial cell motility. *J. Biol. Chem.* **289**, 5904–5913 (2014).
44. Flamme, I., Breier, G. & Risau, W. Vascular endothelial growth factor (VEGF) and VEGF receptor 2 (flk-1) are expressed during vasculogenesis and vascular differentiation in the quail embryo. *Dev. Biol.* **169**, 699–712 (1995).
45. Ferland-McCollough, D., Slater, S., Richard, J., Reni, C. & Mangialardi, G. Pericytes, an overlooked player in vascular pathobiology. *Pharm. Ther.* **171**, 30–42 (2017).
46. Bergers, G. & Song, S. The role of pericytes in blood-vessel formation and maintenance. *Neuro Oncol.* **7**, 452–464 (2005).
47. Grossniklaus, H. E., Kang, S. J. & Berglin, L. Animal models of choroidal and retinal neovascularization. *Prog. Retin Eye Res* **29**, 500–519 (2010).
48. Connor, K. M. et al. Quantification of oxygen-induced retinopathy in the mouse: a model of vessel loss, vessel regrowth and pathological angiogenesis. *Nat. Protoc.* **4**, 1565–1573 (2009).
49. Hu, G., Place, A. T. & Minshall, R. D. Regulation of endothelial permeability by Src kinase signaling: vascular leakage versus transcellular transport of drugs and macromolecules. *Chem. Biol. Interact.* **171**, 177–189 (2008).
50. Aguilar, E. et al. Src kinase inhibition reduces laser or VEGF induced retinal vascular permeability. *Investigative Ophthalmol. Vis. Sci.* **45**, 499–499 (2004).
51. Pe'er, J. et al. Hypoxia-induced expression of vascular endothelial growth factor by retinal cells is a common factor in neovascularizing ocular diseases. *Lab Invest* **72**, 638–645 (1995).
52. Rodrigues, M. et al. VEGF secreted by hypoxic müller cells induces MMP-2 expression and activity in endothelial cells to promote retinal neovascularization in proliferative diabetic retinopathy. *Diabetes* **62**, 3863–3873 (2013).
53. Xu, J. et al. VEGF promotes the transcription of the human PRL-3 gene in HUVEC through transcription factor MEF2C. *PLoS One* **6**, e27165 (2011).
54. Srinivasan, R. et al. Erk1 and Erk2 regulate endothelial cell proliferation and migration during mouse embryonic angiogenesis. *PLoS One* **4**, e8283 (2009).
55. Yang, W. J. et al. Paxillin regulates vascular endothelial growth factor A-induced in vitro angiogenesis of human umbilical vein endothelial cells. *Mol. Med Rep.* **11**, 1784–1792 (2015).
56. Tornavaca, O. et al. ZO-1 controls endothelial adherens junctions, cell-cell tension, angiogenesis, and barrier formation. *J. Cell Biol.* **208**, 821–838 (2015).
57. Vestweber, D. VE-Cadherin. *Arteriosclerosis, Thrombosis, Vasc. Biol.* **28**, 223–232 (2008).
58. Arepalli, S. & Kaiser, P. K. Pipeline therapies for neovascular age related macular degeneration. *Int. J. Retin. Vitreous* **7**, 55 (2021).
59. Dellinger, M. T. & Brekken, R. A. Phosphorylation of Akt and ERK1/2 is required for VEGF-A/VEGFR2-induced proliferation and migration of lymphatic endothelium. *PLoS One* **6**, e28947 (2011).
60. Sun, Z. et al. VEGFR2 induces c-Src signaling and vascular permeability in vivo via the adaptor protein TAd. *J. Exp. Med* **209**, 1363–1377 (2012).
61. Wang, W., Dentler, W. L. & Borchardt, R. T. VEGF increases BMEC monolayer permeability by affecting occludin expression and tight junction assembly. *Am. J. Physiol. -Heart Circulatory Physiol.* **280**, H434–H440 (2001).
62. Funyu, J., Mochida, S., Inao, M., Matsui, A. & Fujiwara, K. VEGF can act as vascular permeability factor in the hepatic sinusoids through upregulation of porosity of endothelial cells. *Biochem Biophys. Res Commun.* **280**, 481–485 (2001).
63. Feng, D. et al. Reinterpretation of endothelial cell gaps induced by vasoactive mediators in guinea-pig, mouse and rat: many are transcellular pores. *J. Physiol.* **504**, 747–761 (1997).
64. Feng, D. et al. Pathways of macromolecular extravasation across microvascular endothelium in response to VPF/VEGF and other vasoactive mediators. *Microcirculation* **6**, 23–44 (1999).
65. Messmer, K. J. & Abel, S. R. Verteporfin for age-related macular degeneration. *Ann. Pharmacother.* **35**, 1593–1598 (2001).
66. Bressler, N. M. & Bressler, S. B. Photodynamic therapy with verteporfin (Visudyne): Impact on ophthalmology and visual sciences. *Investigative Ophthalmol. Vis. Sci.* **41**, 624–628 (2000).
67. Lim, T. H. et al. Comparison of ranibizumab with or without verteporfin photodynamic therapy for polypoidal choroidal vasculopathy: The EVEREST II randomized clinical trial. *JAMA Ophthalmol.* **138**, 935–942 (2020).
68. Michels, S., Rosenfeld, P. J., Puliafito, C. A., Marcus, E. N. & Venkatraman, A. S. Systemic bevacizumab (Avastin) therapy for neovascular age-related macular degeneration twelve-week results of an uncontrolled open-label clinical study. *Ophthalmology* **112**, 1035–1047 (2005).
69. Moshfeghi, A. A. et al. Systemic bevacizumab (Avastin) therapy for neovascular age-related macular degeneration: twenty-four-week results of an uncontrolled open-label clinical study. *Ophthalmology* **113**, 2002–2011.e2002 (2006).

70. Nguyen, Q. D. et al. A phase I trial of an IV-administered vascular endothelial growth factor trap for treatment in patients with choroidal neovascularization due to age-related macular degeneration. *Ophthalmology* **113**, 1522.e1521–1522.e1514 (2006).
71. Ang, K. <https://BioRender.com/avx4snb> (2025).
72. Ang, K. <https://BioRender.com/xeucwcn> (2025).
73. Ang, K. <https://BioRender.com/t9u2tyn> (2025).

Acknowledgements

We would like to acknowledge the assistance from Kim Chi Tran, Dr Sze Yuan Ho and Dr Rui Ning Chia. We sincerely thank Prof Hong Wanjin for his constructive comments in preparation of the manuscript. This research was funded by Institute of Molecular and Cell Biology Core Fund [SC15-R0036] to Q.Z. and Agency for Science, Technology and Research, Career Development Fund [C210812005] to K.H.A. Rabbit toxicology study was funded by Intra-ImmuSG Pte Ltd.

Author contributions

Conceptualization, K.H.A., M.T. and Q.Z.; Study Design, data layouts, original discussion, K.H.A., M.T. and Q.Z.; Writing—review and editing, K.H.A., M.T., P.L.C.; J.M.H., Q.Z. In vitro: K.H.A., K.Y.K and P.L.C; In vivo: Q.S.W.T., K.H.A., M.T., A.G., K.K.Y., J.L., B.Q., X.W. and X.S.; Supervision, Q.Z.; Project administration, Q.Z. All authors have read and agreed to the published version of the manuscript.

Competing interests

Q.Z. is the Founder, K.H.A. is the Chief Operating Officer (recent J.A.), M.T. is the Chief Medical Officer (recent J.A.), and K.K.Y is the Clinical Research Coordinator (recent J.A.) of Intra-ImmuSG Pte Ltd., an Agency for Science, Technology and Research (A*STAR) spin-off company granted licensing rights for the PRL3-zumab IP portfolio. The other authors declare no competing interests. J.A.: Joint Appointment.

Additional information

Supplementary information The online version contains supplementary material available at <https://doi.org/10.1038/s41467-025-59929-2>.

Correspondence and requests for materials should be addressed to Qi Zeng.

Peer review information *Nature Communications* thanks Winfried Amoaku, Yunpeng Bai, Thomas Langmann, and the other, anonymous, reviewer(s) for their contribution to the peer review of this work. A peer review file is available.

Reprints and permissions information is available at <http://www.nature.com/reprints>

Publisher's note Springer Nature remains neutral with regard to jurisdictional claims in published maps and institutional affiliations.

Open Access This article is licensed under a Creative Commons Attribution-NonCommercial-NoDerivatives 4.0 International License, which permits any non-commercial use, sharing, distribution and reproduction in any medium or format, as long as you give appropriate credit to the original author(s) and the source, provide a link to the Creative Commons licence, and indicate if you modified the licensed material. You do not have permission under this licence to share adapted material derived from this article or parts of it. The images or other third party material in this article are included in the article's Creative Commons licence, unless indicated otherwise in a credit line to the material. If material is not included in the article's Creative Commons licence and your intended use is not permitted by statutory regulation or exceeds the permitted use, you will need to obtain permission directly from the copyright holder. To view a copy of this licence, visit <http://creativecommons.org/licenses/by-nc-nd/4.0/>.

© The Author(s) 2025